

and assume that $B_{ij}(q^{-1}) = 0$ for $j > 1$. The principles of Section III indicate that such a structure has lowest complexity. These choices interpret Fig. 5 as a tapped cascade of second-order sections, as shown in Fig. 11. It is shown in [10] that such a structure is able to represent an arbitrary strictly proper transfer function of order $2M$. A proper transfer function may be realized by including a tap directly between u and y .

To implement the i th section, consisting of F_{i1} and the subsequent "tap" transfer function B_{i1} , in lowest complexity form, we apply the concepts given in Section 3. In particular, the sensitivities for the parameters in B_{i1} will be available in its tapped delay line, while the sensitivities for the parameters in F_{i1} can be constructed as discussed below (10). One must be careful, however, to apply the filtering operation of $1/(1 - a_{i1}q^{-1} - a_{i2}q^{-2})$ that is used in the sensitivity generation only to the part of the output y that is influenced by the parameters in the i section. This is the reason why the signals from the taps are summed from right to left in Fig. 11 (as is done for the outputs of B_{ij} in Fig. 5).

The resulting structure showing both the i th section itself and also its associated sensitivity generations is given in Fig. 12. Note that the additional delays present in F_{i1} in (12) do not modify this construction. Notice also that only two additional multipliers occur in the sensitivity generation, indicating the lowest complexity characteristic.

V. CONCLUSION

We have examined in this brief the problem of implementing adaptive IIR filters with lowest complexity, as measured by the number of multiplications used to generate the filter output and additionally the sensitivities with respect to all adapted parameters. We have shown that for an order N filter, the minimum number of such multiplications is $3N + 1$. We outlined some strategies for obtaining a lowest complexity implementation, and applied these to direct-, cascade-, and parallel-form implementations.

REFERENCES

- [1] D. Parikh, N. Ahmed, and S. Stearns, "An adaptive lattice algorithm for recursive filters," *IEEE Trans. Acoust., Speech, Signal Processing*, vol. ASSP-28, pp. 110–111, Feb. 1980.
- [2] G. A. Williamson, C. R. Johnson Jr., and B. D. O. Anderson, "Locally robust identification of linear systems containing unknown gain elements with application to adapted IIR lattice models," *Automatica*, vol. 27, pp. 783–798, May 1991.
- [3] J. A. Rodriguez-Fonollosa and E. Masgrau, "Simplified gradient calculation in adaptive IIR lattice filters," *IEEE Trans. Signal Processing*, vol. 39, pp. 1702–1705, July 1991.
- [4] N. Nayeri and W. K. Jenkins, "Alternate realizations of adaptive IIR filters and properties of their performance surfaces," *IEEE Trans. Circuits Syst.*, vol. 36, pp. 485–496, Apr. 1989.
- [5] B. D. Rao, "Adaptive IIR filtering using cascade structures," in *Proc. 27th Asilomar Conf. Signals, Syst., and Comput.*, Nov. 1993, Pacific Grove, CA, pp. 194–198.
- [6] L. B. Jackson and S. L. Wood, "Linear prediction in cascade form," *IEEE Trans. Acoust., Speech, Signal Processing*, vol. 26, pp. 518–528, Dec. 1978.
- [7] P. A. Regalia, "Stable and efficient lattice algorithms for adaptive IIR filtering," *IEEE Trans. Signal Processing*, vol. 40, pp. 375–388, Feb. 1992.
- [8] A. H. Gray Jr. and J. D. Markel, "Digital lattice and ladder filter synthesis," *IEEE Trans. Audio Electroacoust.*, vol. 21, pp. 491–500, Dec. 1973.

- [9] S. Bingulac, J. H. Chow, and J. R. Winkelman, "Simultaneous generation of sensitivity functions—Transfer function matrix approach," *Automatica*, vol. 24, pp. 239–242, Feb. 1988.
- [10] G. A. Williamson and S. Zimmermann, "Globally convergent adaptive IIR filters based on fixed pole locations," *IEEE Trans. Signal Processing*, vol. 44, pp. 1418–1427, June 1996.

On the Common Mode Rejection Ratio in Low Voltage Operational Amplifiers with Complementary N-P Input Pairs

Fan You, Sherif H. K. Embabi, and Edgar Sánchez-Sinencio

Abstract—Low voltage op amps with complementary N-P input differential pairs are known to suffer from low common mode rejection ratio due to mismatch errors and the tail current switching between the N and P input stage. To understand the contribution of the systematic and the random common mode gains to the overall common mode rejection ratio (CMRR) we studied three op amp topologies, which use N-P complementary input differential pairs. A detailed small signal analysis for each of them has been performed to compare their systematic and random CMRR. The analysis shows that random CMRR caused by mismatch does not depend on the topology, while the systematic CMRR is topology dependent. It is also concluded that the CMRR of low voltage op amps with N-P complementary input pairs will be ultimately limited by the process mismatch and that the random CMRR will determine the overall CMRR.

Index Terms—Common mode rejection ratio (CMRR), low voltage, operational amplifier.

I. INTRODUCTION

There is a strong demand for lowering the supply voltage of analog circuits including op amps. To increase the signal to noise ratio of low voltage op amps, it is highly desirable to have a rail-to-rail input voltage swing. N-P complementary pairs have been widely used in the input stage of low voltage op amps to achieve a rail-to-rail input voltage swing [1]–[8]. An advantage of using N-P complementary differential pairs is that the op amps can be implemented in a standard digital process. Fig. 1 shows a typical structure of a low voltage op amp with N-P differential pairs. Using N-P complementary input pairs will, however, degrade the common mode rejection ratio (CMRR). This occurs while the tail current switches between the P and N pairs. A CMRR as low as 40–55 dB has been reported in [4], [6], and [7]. This brief presents a rigorous analysis of the CMRR of low voltage op amps with N-P differential pairs. Three illustrative topologies have been considered here. In Section II, a derivation of the CMRR of the three op amp topologies with complementary N-P pairs is presented. In Section III, we compare the systematic and random CMRR of the different topologies. The random CMRR is compared with the systematic CMRR in Section IV, to find which

Manuscript received October 31, 1995; revised April 5, 1996. This paper was recommended by Associate Editor F. Larsen.

F. You was with the Department of Electrical Engineering, Texas A&M University, College Station, TX 77843 USA. He is now with Bell Laboratories, Lucent Technologies, Allentown, PA 18103 USA.

S. H. K. Embabi and E. Sánchez-Sinencio are with the Department of Electrical Engineering, Texas A&M University, College Station, TX 77843 USA.

Publisher Item Identifier S 1057-7130(97)03654-9.

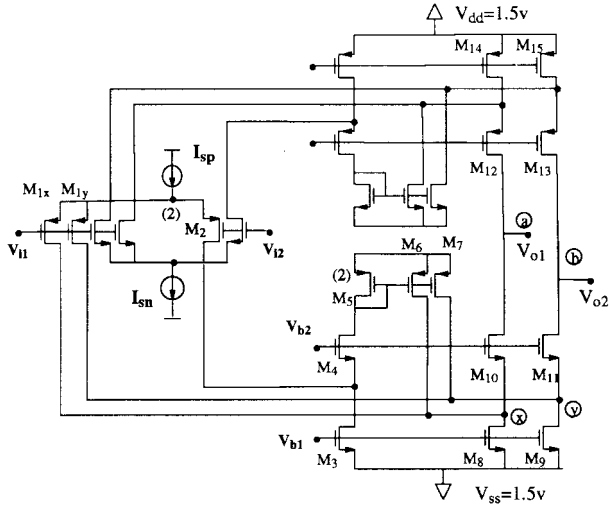


Fig. 1. An N-P complementary input stage with common mode cancellation proposed in [1]—Topology I.

of them determines the overall CMRR for each of the topologies under consideration. Finally, we verify the results of the analysis with simulation and study the CMRR as a function of frequency.

II. DERIVATION OF COMMON MODE GAIN OF THE LOW VOLTAGE OP AMP

The use of N-P complementary input pairs to achieve rail to rail input swing may result in a variable transconductance of the input stage—a property which severely affects the optimal compensation of the op amp. In order to make the overall g_m constant, the tail currents I_{sn} and I_{sp} (in Fig. 1) are generated using a square-root current source which maintains the sum of the square root of both currents constant ($\sqrt{I_{sn}} + \sqrt{I_{sp}} = \text{constant}$) [1], [4]. If the input devices of the differential pair operate in the weak inversion region, a current source which maintains the sum of the two tail currents constant ($I_{sn} + I_{sp} = \text{constant}$) [5], [6] is used to achieve a constant g_m . The tail currents I_{sp} and I_{sn} are, however, dependent on the common mode input voltage (V_{cm}) as illustrated in Fig. 2. Both currents exhibit sharp changes in magnitude as the tail current switches between the N and the P pair. Although the g_m may be constant, the CMRR is not. Fig. 2 shows the simulation result of using a constant- g_m input stage with a square-root current source. A drop of at least 35 dB in the CMRR can be observed. For the N-channel input stage, as V_{cm} is lowered toward V_{ss} , the NMOS which is acting as the current source is pushed into triode region. This means that the resistance of the current source decreases and that the common mode gain increases. If V_{cm} is further lowered, the N-pair is completely turned off and it will not contribute to the overall common mode gain. A similar explanation applies for the P stage, and we will have an increase in common mode gain when either current source operates in the triode region.

In the following subsections, we present a detailed analysis of the small signal differential and common mode gains of three op amp topologies. All three have N-P complementary differential pairs. The second stage is different for each topology. The first and the second topology (Figs. 1 and 5) have been reported in [1]–[3], respectively. We are proposing a third topology (Fig. 6) which is basically an improved version of the second topology shown in Fig. 5. For each circuit, we will derive the systematic CMRR, which is topology dependent, and the random CMRR, which is a function of the process mismatching.

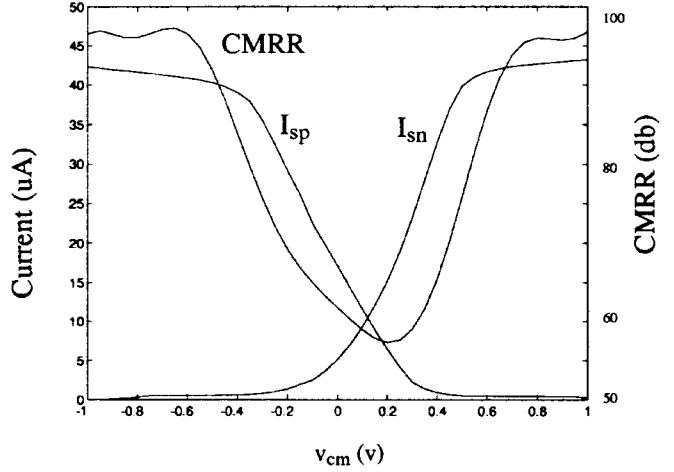


Fig. 2. CMRR and tail current I_{sn} and I_{sp} versus V_{cm} .

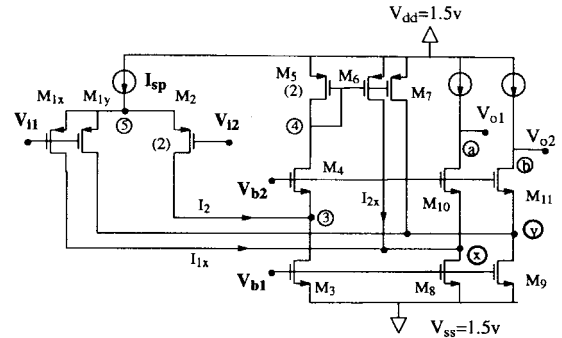


Fig. 3. The half of the amplifier of Fig. 1 used for small signal analysis.

A. Topology I

The circuit topology shown in Fig. 1 has a special circuit (M_4 – M_7) whose function is to cancel the common mode current resulting from the change of the tail current [1]. For the common mode gain analysis, we will consider only one input pair as shown in Fig. 3. For the N-P complementary input amplifiers, the overall small signal gain is simply the summation of the gains of the two input pairs. The tail current I_{sp} in the figure is assumed to be generated by a constant- g_m current biasing circuit. To maintain generality, we use a generic model for the tail current generator I_{sp} in the small signal analysis. Since the value of the tail current is dependent on the common mode input voltage v_{cm} , we may use a voltage controlled current source $G_{ms}v_{cm}$ as its ac model. Note that G_{ms} is a function of the dc common mode input voltage. The finite output conductance of the I_{sp} current source is also accounted for through the use of g_{os} as shown in Fig. 4. The conductance seen through the source of M_{10} and M_{11} in Fig. 3 has been modeled as g_{ex} and g_{ey} as shown in Fig. 4. The conductance g_{ex} and g_{ey} are fairly low because the resistance of the loads connected to nodes a and b are very large. It can be shown that g_{ex} and g_{ey} are in the order of g_o ($1/r_{ds}$) and not g_m as expected for small load resistance [9].

Note that the following analyses are carried out for the range of V_{cm} where the tail currents (I_{sp} and I_{sn}) are switching. It is in this current transition range where the CMRR becomes minimum.

In the CMRR analysis the input voltages v_{i1} and v_{i2} are usually expressed as functions of the differential and common mode inputs:

$$v_{i1} = v_{cm} - \frac{1}{2} v_{dm} \quad (1a)$$

$$v_{i2} = v_{cm} + \frac{1}{2} v_{dm}. \quad (1b)$$

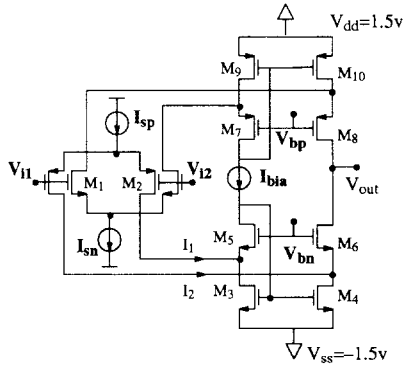


Fig. 5. An op amp with N-P complementary differential pairs [2], [3]—Topology II.

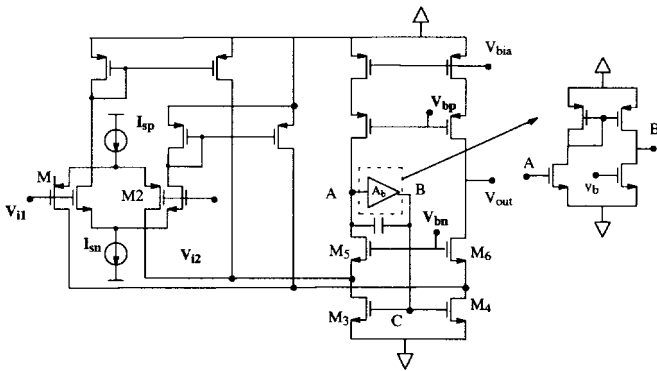


Fig. 6. A low voltage amplifier with systematic CMRR enhancement—Topology III.

improves by A_b as shown by the following equation:

$$\text{CMRR}_s \approx A_b \frac{2g_{m2} g_{m4} g_{m6}}{G_{ms} g_{o6} (g_{o2} + g_{o4})}. \quad (11)$$

The random CMRR, however, remains unchanged and is given by

$$\text{CMRR}_r \approx \frac{2g_{m2}}{\epsilon G_{ms}}. \quad (12)$$

III. COMPARISON OF THE CMRR OF THE THREE TOPOLOGIES

Although each of the topologies has a scheme for systematic common mode current cancellation, yet, the accuracy of the cancellation varies. In the first topology (Fig. 3), the common mode current I_{1x} is supposed to be cancelled out through I_{2x} which is half of the common mode current I_2 . This is only true if all of I_2 is injected into M_4 . Due to the finite conductance (g_{o3}) of M_3 , I_{2x} will be slightly less than $I_2/2$. Thus the cancellation is not exact even if the mirror transistors M_5 and M_6 are perfectly matched. In the case of the second topology (Fig. 5), if we assume perfect matching between M_3 and M_4 , it can be easily seen that the common mode current I_2 will be exactly cancelled by the mirror of I_1 . A similar explanation can be given for Topology III. It is, hence, expected that the common mode cancellation of Topologies II and III is more accurate than that of Topology I. This implies that the systematic CMRR of II and III will be superior to that of I which is confirmed by the analytical expressions derived in Section II and summarized in Table I.

The similarity of CMRR_r of the three different topologies can be explained by using a more general amplifier model which is illustrated in Fig. 7. In the figure, the block " $I_2 - I_1$ " is an abstract model for the cancellation of the common mode current due to G_{ms} . A common mode input (v_{cm}) will generate a tail current $I_{sp} = G_{ms} v_{cm}$.

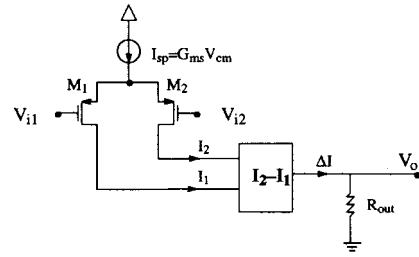


Fig. 7. A general amplifier model with tail current variation and common mode cancellation.

Assuming that there is mismatch (ϵ) in the input differential pair [i.e., $g_{m2} = g_{m1}(1 + \epsilon)$], the current in the two input transistors could be expressed as $I_1 = G_{ms} v_{cm}/2$ and $I_2 = G_{ms} v_{cm}(1 + \epsilon)/2$. The difference between the currents of the two input transistors due to $G_{ms} v_{cm}$ can be written as: $\Delta I_{cm} = \epsilon G_{ms} v_{cm}/2$. A differential input v_{dm} will otherwise generate the following current difference: $\Delta I_{dm} = g_m v_{dm}$, where g_m is the transconductance of the input pair. Since the differential and common mode output voltages are given by $\Delta I_{dm} R_{out}$ and $\Delta I_{cm} R_{out}$, respectively, we can derive the following generic expression for the random CMRR:

$$\text{CMRR}_r = \frac{A_{dm}}{A_{cm}} = \frac{2g_m}{\epsilon G_{ms}}$$

which is the same as (7), (10), and (12). This simple analysis confirms that the CMRR_r is topologies independent.

IV. COMPARISON BETWEEN SYSTEMATIC CMRR AND RANDOM CMRR

It is interesting to note that both the systematic and the random common mode rejection ratios are reciprocally proportional to the common mode transconductance (G_{ms}). To compare between CMRR_s and CMRR_r , we first need to compare the magnitude of G_{ms} with that of g_o 's and g_m 's. G_{ms} is the rate of change of I_{sp} (or I_{sn}) when I_{sp} and I_{sn} are switching. The expression of G_{ms} is $I_{max}/(V_{dd} - V_{ss})\alpha$, where I_{max} is the maximum value of I_{sp} (or I_{sn}) and α is typically 0.5 or less (see Fig. 2). The typical value of g_o is in the order of λI_{max} . Hence

$$\frac{G_{ms}}{g_o} \approx \frac{1}{\lambda \alpha (V_{dd} - V_{ss})}.$$

For $\lambda = 0.01$ and $V_{dd} = -V_{ss} = 1.5$ V and $\alpha = 0.5$, $G_{ms}/g_o \approx 67$. G_{ms} and g_m are of comparable magnitudes. So, we may assume that

$$g_o < G_{ms} \leq g_m. \quad (13)$$

Let us first ignore the mismatching. The minimum common mode rejection is determined by the systematic common mode gain. Using the inequality (13) we can determine the order of the CMRR_s for all three topologies as shown in Table I. For Topology I, the CMRR_s is in the order of $g_m^2/G_{ms}g_o$ (25–35 dB), the CMRR_s of the second topology is in the order of $g_m^3/G_{ms}g_o^2$ (50–70 dB). The third topology may have a CMRR_s of the order of 70–95 dB. For a typical mismatching factor (ϵ) less than 1% [11], the CMRR_r is close to 40–60 dB.

For all three topologies, we now compare the CMRR_s with CMRR_r to evaluate which of the two components limit the improvement of CMRR. The ratios of $\text{CMRR}_s/\text{CMRR}_r$ for all topologies is summarized in Table I. For the first topology (Fig. 1), the ratio is less than unity, which implies that the overall CMRR will be determined by the low systematic CMRR. In the case of the second topology, the CMRR_s approaches the CMRR_r . As for the third topology, the

TABLE I
COMPARISON OF RANDOM AND SYSTEMATIC CMRR

CMRR / Topology	I	II	III
$CMRR_s$	$\frac{2g_{m2}g_{m4}}{G_{ms}(g_{o2} + g_{o3})}$ $O\left(\frac{g_m^2}{G_{ms}g_o}\right) \approx 25\text{--}35$ dB	$\frac{2g_{m2}g_{m4}g_{m6}}{G_{ms}g_{o6}(g_{o2} + g_{o4})}$ $O\left(\frac{g_m^3}{G_{ms}g_o^2}\right) \approx 50\text{--}75$ dB	$\frac{2A_b g_{m2}g_{m4}g_{m6}}{G_{ms}g_{o6}(g_{o2} + g_{o4})}$ $O\left(\frac{A_b g_m^3}{G_{ms}g_o^2}\right) \approx 70\text{--}95$ dB
$CMRR_r$	$\frac{2g_{m2}}{\epsilon G_{ms}}$ $O\left(\frac{2}{\epsilon}\right) \approx 40\text{--}60$ dB	$\frac{2g_{m2}}{\epsilon G_{ms}}$ $O\left(\frac{2}{\epsilon}\right) \approx 40\text{--}60$ dB	$\frac{2g_{m2}}{\epsilon G_{ms}}$ $O\left(\frac{2}{\epsilon}\right) \approx 40\text{--}60$ dB
$\frac{CMRR_s}{CMRR_r}$	$\frac{\epsilon g_{m2}}{(g_{o2} + g_{o3})} < 1$	$\frac{\epsilon g_{m4}g_{m6}}{g_{o6}(g_{o2} + g_{o4})} \geq 1$	$\frac{A_b \epsilon g_{m4}g_{m6}}{g_{o6}(g_{o2} + g_{o4})} > 1$

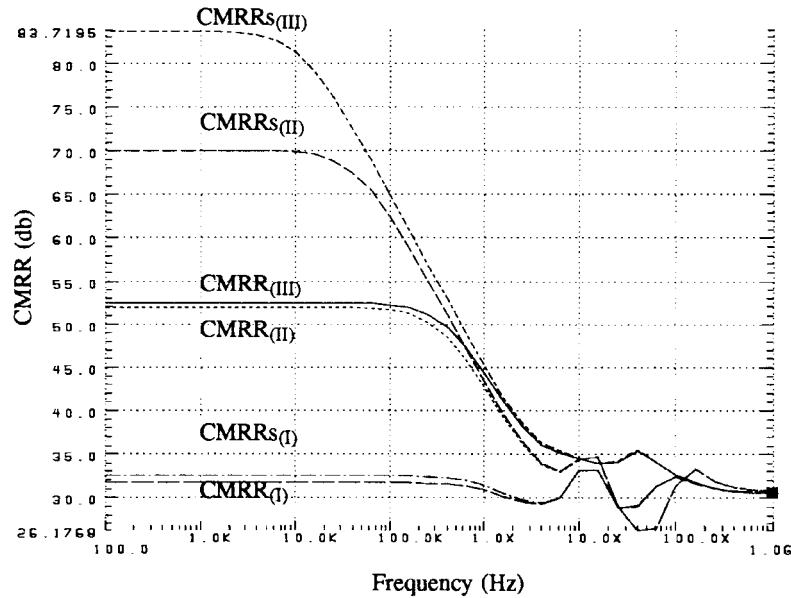


Fig. 8. CMRR versus frequency with and without mismatching.

systematic CMRR exceeds the random CMRR, hence, the overall CMRR will be determined by the $CMRR_r$.

V. SIMULATION RESULTS

To verify the results of the above analysis, the CMRR of all the three topologies has been simulated using HSPICE. The three amplifiers were designed to have the same gain bandwidth product of 3 MHz with 10 pF of capacitive load and the same low frequency differential gain. First the systematic CMRR was simulated assuming no mismatches. The result of the simulations are depicted in Fig. 8. Note that the curves denoted as $CMRR_s$ (I), $CMRR_s$ (II), and $CMRR_s$ (III) represent the systematic CMRR for Topologies I, II, and III, respectively. From these three curves we can make the following observations. First, the low frequency $CMRR_s$ of Topology I is the lowest with 32 dB, the $CMRR_s$ of Topology II is 70 dB, and that of Topology III is the largest with 84 dB. These numbers agree with the theoretical analysis (see Table I). The second observation is that the systematic CMRR of Topologies II and III drops beyond 10 kHz, but is still greater than that of Topology I even at 3 MHz. The advantage of II and III over I in terms of $CMRR_s$, however, gradually diminishes as the frequency increase. To study the effect of mismatching, the simulation was performed with 2% mismatch in the input pair. The simulated total CMRR, which includes systematic and random CMRR, is also shown in Fig. 8 as $CMRR$ (I), $CMRR$ (II)

and $CMRR$ (III). It is interesting to note that Topologies II and III have similar CMRR which is smaller than their systematic CMRR. This confirms that the CMRR of these two topologies will be limited by the random CMRR which is equal for all three topologies. As for the first amplifier, the $CMRR_s$ is smaller than $CMRR_r$, and therefore the total CMRR is slightly smaller than $CMRR_s$.

The above theoretical analysis and simulation all confirm that the systematic CMRR can be improved through topology modification. By doing that, the random common mode gain becomes the ultimate factor to determine the overall CMRR. The effect of mismatching on the simulated CMRR for the circuits in Figs. 5 and 6 is illustrated in Fig. 9. It is observed that the CMRR of the circuit in Fig. 6 is much greater than that in Fig. 5, when the mismatching is small (below 0.1%). However, this is hardly realizable in practical amplifiers. The topology with the systematic CMRR enhancement is useful only if the transistor matching is very good. It is also observed from the figure that both circuits have similar CMRR when the matching is poor since the typical mismatching factor (ϵ) is in the order of 0.1% or more. It is expected that mismatching will be the dominant factor in determining the CMRR.

VI. CONCLUSION

In this brief, the CMRR degradation problem in low voltage op amps with N-P complementary pairs is discussed. A small signal

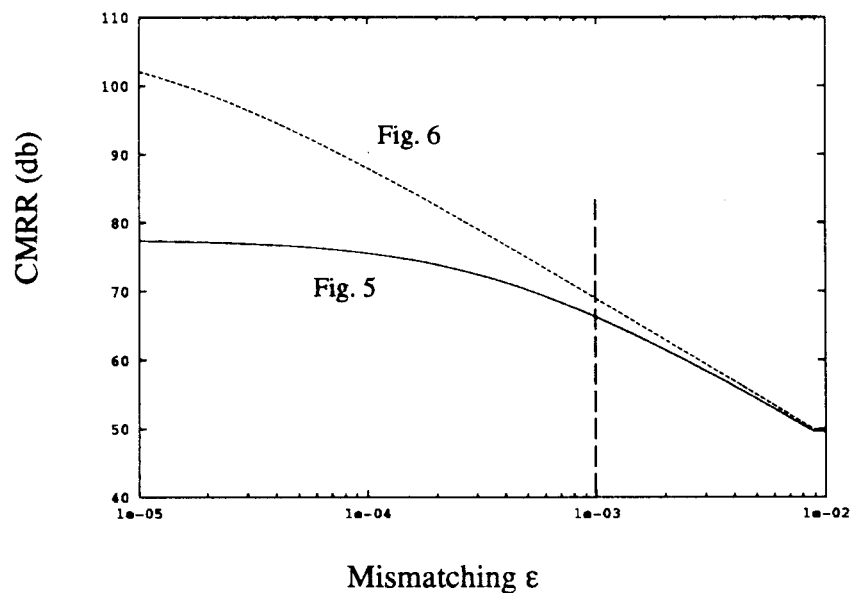


Fig. 9. Effect of mismatching on the CMRR.

analysis revealed that the increase of both systematic and mismatching common mode gain in the low voltage op amp is due to the change of the tail current of the N–P complementary pairs. The systematic CMRR degradation can be improved by using suitable topologies. However the common mode gain due to mismatching remains to be a dominant factor which limits the CMRR improvement.

REFERENCES

- [1] J. H. Botma, R. F. Wassenaar, and R. J. Wiegink, "A low-voltage CMOS op amp with a rail-to-rail constant- g_m input stage and a class AB rail-to-rail output stage," in *IEEE 1993 ISCAS*, Chicago, IL, pp. 1314–1317.
- [2] R. Hogervorst, J. P. Tero, R. G. H. Eschauzier, and J. H. Huijsing, "A compact power-efficient 3 V CMOS rail-to-rail input/output operational amplifier for VLSI cell libraries," in *ISSCC*, Feb. 1994, pp. 244–245.
- [3] W. S. Wu, W. J. Helms, J. A. Kuhn, and B. E. Byrket, "Digital-compatible high-performance operational amplifier with rail-to-rail input and output ranges," *IEEE J. Solid-State Circuits*, vol. 29, pp. 63–66, Jan. 1994.
- [4] J. F. Duque-Carrillo, R. Perez-Aloe, and J. M. Valverde, "Biasing circuit for high input swing operational amplifiers," *IEEE J. Solid-State Circuits*, vol. 30, pp. 156–159, Feb. 1995.
- [5] J. F. Duque-Carrillo, J. M. Valverde, and R. Perez-Aloe, "Constant- g_m rail-to-rail common-mode range input stage with minimum CMRR degradation," *IEEE J. Solid-State Circuits*, vol. 28, pp. 661–666, June 1993.
- [6] M. D. Pardo and M. G. Degrauwe, "A rail-to-rail input/output CMOS power amplifier," *IEEE J. Solid-State Circuits*, vol. 25, pp. 501–504, Apr. 1990.
- [7] R. Hogervorst *et al.*, "CMOS low-voltage operational amplifiers with constant- g_m rail-to-rail input stage," in *Proc. ISCAS*, 1992, pp. 2876–2879.
- [8] M. Ismail and T. Fiez, *Analog VLSI Signal and Information Processing*. New York: McGraw-Hill, 1994.
- [9] K. Laker and W. Sansen, *Design of Analog Integrated Circuits and Systems*. New York, 1994.
- [10] B. Char *et al.*, *Maple V Library Reference Manual*. New York: Springer-Verlag, 1991.
- [11] J. Franca and Y. Tsividis, *Design of Analog-Digital VLSI Circuits for Telecommunication and Signal Processing*. Englewood Cliffs, NJ: Prentice-Hall, 1994.